

# Thermodynamics of Ising spins on the triangular kagome lattice: Exact analytical method and Monte Carlo simulations

Y. L. Loh, D. X. Yao, and E. W. Carlson

Department of Physics, Purdue University, West Lafayette, IN 47907

(Dated: November 22, 2007)

A new class of two-dimensional magnetic materials  $\text{Cu}_9\text{X}_2(\text{cpa})_6 \cdot x\text{H}_2\text{O}$  (cpa=2-carboxypentonic acid;  $\text{X}=\text{F}, \text{Cl}, \text{Br}$ ) was recently fabricated in which Cu sites form a Triangular Kagome Lattice (TKL). As the simplest model of geometric frustration in such a system, we study the thermodynamics of Ising spins on the TKL using exact analytic methods as well as Monte Carlo simulations. We present the free energy, internal energy, specific heat, entropy, sublattice magnetizations, and susceptibility. We describe the rich phase diagram of the model as a function of coupling constants, temperature, and applied magnetic field. For frustrated interactions in the absence of applied field, the ground state is a spin liquid phase with residual entropy per spin  $s_0/k_B = \frac{1}{9} \ln 72 \approx 0.4752 \dots$ . In weak applied field, the system maps to the dimer model on a honeycomb lattice, with residual entropy 0.0359 per spin and quasi-long-range order with power-law spin-spin correlations that should be detectable by neutron scattering. The power-law correlations become exponential at finite temperatures, but the correlation length may still be long.

PACS numbers: 75.30.Kz, 75.40.Mg, 75.10.Hk, 64.60.-i

## I. INTRODUCTION

Geometrically frustrated spin systems give rise to many novel classical and quantum spin liquid phases. They may have technological applications as refrigerants, via adiabatic demagnetization,<sup>1</sup> in which reducing the applied magnetic field results in a cooling effect as the spins absorb entropy from other degrees of freedom. Unlike paramagnetic salts which are limited by ordering or spin-glass transitions due to residual interactions between the spins, geometrically frustrated systems can remain in a disordered, cooperative paramagnetic state down to the lowest temperatures. Furthermore, they may exhibit an enhanced magnetocaloric effect in the vicinity of phase transitions at finite applied fields.<sup>2,3,4,5</sup>

A new class of two-dimensional magnetic materials  $\text{Cu}_9\text{X}_2(\text{cpa})_6 \cdot x\text{H}_2\text{O}$  (cpa=2-carboxypentonic acid, a derivative of ascorbic acid;  $\text{X}=\text{F}, \text{Cl}, \text{Br}$ )<sup>6,7,8</sup> was recently fabricated, which is an experimental realization of a new type of geometrically frustrated lattice. The Cu spins in these materials are interconnected in a “triangles-in-triangles” kagome pattern, which we refer to as a triangular kagome lattice (TKL, see Fig. 1).

Experiments on the  $\text{Cu}_9\text{X}_2(\text{cpa})_6 \cdot x\text{H}_2\text{O}$  compounds show no spontaneous magnetization down to at least  $T = 1.7\text{K}$ ,<sup>7</sup> consistent with a spin liquid ground state, indicating that  $J_{aa}$  is antiferromagnetic. However, whether  $J_{ab}$  is ferromagnetic or antiferromagnetic is still an open question. Based on the observation of a partial rather than saturated magnetization,<sup>7,8</sup> Maruti *et al.* concluded that the intertrimer coupling is antiferromagnetic,  $J_{ab} < 0$ .<sup>7</sup> In a later theoretical study using variational mean field theory on the quantum Heisenberg model on the TKL, Strečka<sup>9</sup> concluded that the intertrimer coupling is ferromagnetic,  $J_{ab} > 0$ . Regardless, the lack of observed hysteresis despite the observation of a magnetization plateau in finite field<sup>7</sup> is consistent with a multi-

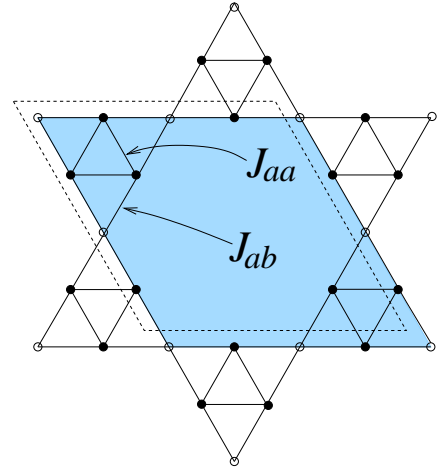


FIG. 1: (Color online) The triangular kagome lattice (TKL). Solid (open) circles represent “a” (“b”) sublattices. Thick and thin lines represent interactions  $J_{aa}$  and  $J_{ab}$  respectively. The shaded region represents a unit cell. By shifting the cell slightly (as indicated by the dashed parallelogram) it can be seen that there are nine spins per unit cell.

tude of ground states which can be connected by a series of local spin flips.

In this paper we study the classical TKL Ising model using exact analytic methods and Monte Carlo simulations. The purpose of this study is to provide explicit predictions, in order to determine to what extent the experiments can be explained in terms of a classical Ising model. In particular, we find significant difference between the behavior of the susceptibility as a function of temperature for  $J_{ab} > 0$  and  $J_{ab} < 0$ , and this may be used as an experimental means of distinguishing the two cases. Discrepancies between experiments and our theoretical predictions will indicate the vector nature of the actual spins (XY or Heisenberg), the effects of quantum

fluctuations, or possibly higher order interactions. This model was previously studied by one of us<sup>10</sup>. In that work, Monte Carlo simulations were used to study the phase transitions and basic thermodynamics. Zheng and Sun<sup>11</sup> mapped the partition function to that of a kagome lattice and found an analytic expression for the phase boundary in zero field.

In this paper we present exact results in zero field at finite temperature, and also in an applied field at zero temperature. We report the full phase diagram as a function of coupling constants, temperature, and applied magnetic field. We find several field-induced transitions. In particular, for frustrated interactions in applied field, we find a quasi-long-range ordered phase which maps to hardcore dimers on the honeycomb lattice. We complement these exact analytic results with Monte Carlo simulations on the magnetization and susceptibility. We report the temperature-dependence of the magnetic susceptibility, and show how it can be used to deduce the sign of the coupling constants.

The paper is organized as follows. The TKL Ising model is described in Section II. In Section III, we present exact results for the TKL Ising model in zero field. In Section IV we present exact results at zero temperature. In Section V we present the phase diagram and describe the various phases. In Section VI we present Monte Carlo results for the susceptibility, spontaneous magnetization, and magnetization curves. In Section VII we compare our model to models of geometrically frustrated magnets on other lattices, as well as to experiments on TKL systems. In Section VIII we present our conclusions, and in Appendix we present two mean-field approximations in order to illustrate their failure in the frustrated regime.

## II. MODEL

The TKL (Fig. 1) can be obtained by inserting triangles inside the triangles of the kagome lattice, for which it is sometimes referred to in the literature as the “triangles-in-triangles” kagome lattice. Alternatively, it can be derived from the triangular lattice by periodically deleting seven out of every sixteen lattice sites. This structure has two different spin sublattices “a” and “b”, which correspond to small trimers and large trimers, respectively. We study Ising spins on the TKL with two kinds of nearest-neighbor interactions, the “intratrimer” couplings  $J_{aa}$  and the “intertrimer” couplings  $J_{ab}$ . Each spin has four nearest neighbors. The Hamiltonian is

$$H = -J_{aa} \sum_{i,j \in a} \sigma_i \sigma_j - J_{ab} \sum_{i \in a, j \in b} \sigma_i \sigma_j - h \sum_i \sigma_i \quad (1)$$

where  $\sigma_i = \pm 1$ , summations run over the nearest spin pairs and all spin sites,  $h$  is an external magnetic field. The shaded region in Fig. 1 is one unit cell, which contains 6  $a$ -spins, 3  $b$ -spins, 6  $a$ - $a$  bonds, and 12  $a$ - $b$  bonds. We shall use  $N_a$  and  $N_b$  to denote the total numbers of

spins on the  $a$  and  $b$  sublattices, so that  $N_a : N_b = 2 : 1$ . The space group of the TKL is the same as that of the hexagonal lattice,  $p6m$ , in Hermann-Mauguin notation.

There are four energy scales in the problem:  $J_{aa}$ ,  $J_{ab}$ ,  $T$ , and  $h$ . We have found it most convenient to take  $|J_{ab}|$  as the unit of energy. Thus, the model can be described by a three-dimensional phase diagram in the space of the three dimensionless parameters  $J_{aa}/|J_{ab}|$ ,  $h/|J_{ab}|$ , and  $T/|J_{ab}|$ . The phase diagram also depends on the sign of  $J_{ab}$ .

## III. EXACT RESULTS IN ZERO FIELD

In this section we present exact analytic results for the TKL Ising model in zero magnetic field ( $h = 0$ ), including the free energy, internal energy, specific heat, and entropy. We use a sequence of  $\nabla$ - $Y$  transformations and series reductions (shown in Fig. 2) to transform the Ising model on a TKL into one on a honeycomb lattice, and then use the known solution for the honeycomb lattice. (See Ref. 11 for a similar analysis that transforms the TKL to a kagome lattice keeping the overall value of the partition function unchanged.) We remark that frustrated Ising models with quenched bond disorder may be studied by *numerical* application of  $\nabla$ - $Y$  and  $Y$ - $\nabla$  transformations<sup>12,13</sup> and/or Pfaffian methods<sup>14</sup>. Our results from this section are plotted in Figs. 5 and 6, using the analytic formulas below (as well as series approximations for extreme values of  $T$ ). These thermodynamic quantities do not depend on the sign of  $J_{ab}$ .

### A. Effective coupling on the equivalent honeycomb lattice

If an Ising model is on a particular lattice contains a spin  $\sigma_0$  connected to only two other spins  $\sigma_1$  and  $\sigma_2$  via couplings  $J_1$  and  $J_2$ , then we can ‘integrate out’  $\sigma_0$  while preserving the value of the partition function, in order to obtain an effective coupling  $J_{12}$ . The transformation also produces a constant factor multiplying the partition function,  $A$ . That is,

$$\sum_{\sigma_0=-1}^{+1} e^{\beta(J_1 \sigma_1 \sigma_0 + J_2 \sigma_2 \sigma_0)} = A e^{\beta J_{12} \sigma_1 \sigma_2} \quad (2)$$

for all combinations of values of  $\sigma_1$  and  $\sigma_2$ . It is most convenient to write the effective coupling in terms of  $t_1, t_2, t_{12}$  where  $t_i = \tanh \beta J_i$ , and the partition function changes in terms of  $x_1, x_2, x_{12}$  where  $x_i = e^{-2\beta J_i}$ :

$$t_{12} = t_1 t_2 \quad (3)$$

$$A = (1 + x_1 x_2) \sqrt{\frac{x_{12}}{x_1 x_2}} \quad (4)$$

The  $x$ ’s and  $t$ ’s are related by Möbius duality transformations,  $x_i = (1 - t_i)/(1 + t_i)$  and  $t_i = (1 - x_i)/(1 + x_i)$ .

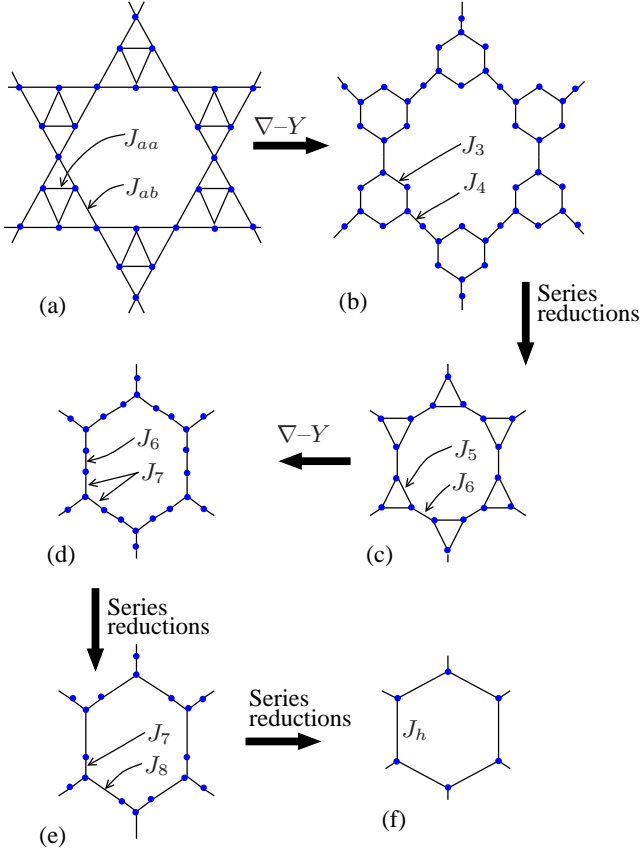


FIG. 2: (Color online). Transformation of a triangular kagome lattice (TKL) to a honeycomb lattice. Figure (a) depicts a section of the TKL, with couplings  $J_{aa}$  and  $J_{ab}$ . The procedure begins by applying  $\nabla$ -Y transformations to the six downward-pointing triangles in each unit cell. This gives lattice (b). Now take the two strong bonds ( $J_3$ ) in series to give  $J_5$ , and the two weak bonds ( $J_4$ ) in series to give  $J_6$ , to obtain a “3-12 lattice” (c). Apply  $\nabla$ -Y transformations to the triangles to obtain a decorated honeycomb lattice (d). Finally, perform series reductions to obtain the honeycomb lattice (f) with a single coupling  $J_h$ .

Similarly, if a spin  $\sigma_0$  is connected to only three other spins  $\sigma_{1,2,3}$  via couplings  $J_{1,2,3}$ , we can ‘integrate out’  $\sigma_0$  while preserving the partition function, in order to obtain effective couplings  $J_{23,31,12}$  together with a free energy shift. This is known as a star-triangle or Y- $\nabla$  transformation. The reverse transformation exists, and is known as a  $\nabla$ -Y transformation: given a “ $\nabla$ ” of couplings  $J_{23,31,12}$ , we can find an equivalent “Y”. Again, it is convenient to use the variables  $t_1 = \tanh \beta J_1$  (and similarly for  $t_2, t_3$ ) and  $x_1 = e^{-2\beta J_1}$ :

$$t_1 = \frac{\sqrt{a_1 a_2 a_3 / a_0}}{a_1} \quad (\text{cycl.}) \quad (5)$$

where

$$a_0 = 1 + t_{23} t_{31} t_{12} \quad (6)$$

$$a_1 = t_{23} + t_{31} t_{12} \quad (\text{cycl.}) \quad (7)$$

$$A = \frac{1}{1 + x_1 x_2 x_3} \sqrt{\frac{x_1 x_2 x_3}{x_{23} x_{31} x_{12}}}, \quad (8)$$

and “cycl.” means that  $t_2, t_3, a_2$ , and  $a_3$  are found by cyclic permutation of the indices 1, 2, 3. In general the  $a$ ’s may be negative or complex-valued, so that it is not correct to replace  $\sqrt{a_1 a_2 a_3 / a_0} / a_1$  by  $\sqrt{a_2 a_3 / a_0 a_1}$ .

Using a sequence of  $\nabla$ -Y transformations and series reductions, we transform the TKL Ising model (with couplings constants  $J_{aa}$  and  $J_{ab}$ ) into a honeycomb Ising model (with a single coupling constant  $J_h$ ), as shown in Fig. 2. The transformation equations (in terms of the  $t_i = \tanh \beta J_i$  variables) are:

$$t_3 = \sqrt{(t_{aa} + t_{ab}^2) / (1 + t_{aa} t_{ab}^2)} \quad (9)$$

$$t_4 = (t_{ab} + t_{aa} t_{ab}) / \sqrt{(t_{aa} + t_{ab}^2)(1 + t_{aa} t_{ab}^2)} \quad (10)$$

$$t_5 = t_3^2 \quad (11)$$

$$t_6 = t_4^2 \quad (12)$$

$$t_7 = 1 / \sqrt{(t_5 + t_5^{-1} - 1)} \quad (13)$$

$$t_8 = t_6 t_7 \quad (14)$$

$$t_h = t_8 t_7 \quad (15)$$

We can write  $t_h$  directly in terms of  $t_{aa}$  and  $t_{ab}$ :

$$t_h = \frac{(1 + t_{aa})^2 t_{ab}^2}{(1 - t_{aa} + t_{aa}^2)(1 + t_{ab}^4) - (1 - 4t_{aa} + t_{aa}^2)t_{ab}^2} \quad (16)$$

It will be convenient to rewrite this in terms of  $x_i = e^{-2\beta J_i}$ , as this is simpler:

$$x_h = \frac{2(3x_{aa}^2 + 1)x_{ab}^2}{x_{ab}^4 + 6x_{aa}^2 x_{ab}^2 + 1} \quad (17)$$

For Ising models, both the triangular lattice and the kagome lattice can be transformed into the honeycomb lattice by a similar procedure. Figure 3 shows the effective dimensionless coupling of the honeycomb lattice,  $\beta J_h$ , as a function of the inverse temperature for antiferromagnetic Ising models on different lattices for comparison. Note that:

- For the triangular Ising AF (TIAF), the effective honeycomb coupling is imaginary, and there is no long-range order.
- For the kagome Ising AF (KIAF), the effective honeycomb coupling is real. As the kagome couplings are increased, the effective honeycomb coupling increases until it saturates at large  $\beta$ . However, it never grows beyond the critical coupling for the honeycomb model,  $\beta J_h^c = \tanh^{-1} 1/\sqrt{3} \approx 0.658$ . Therefore the KIAF does not have a phase transition.

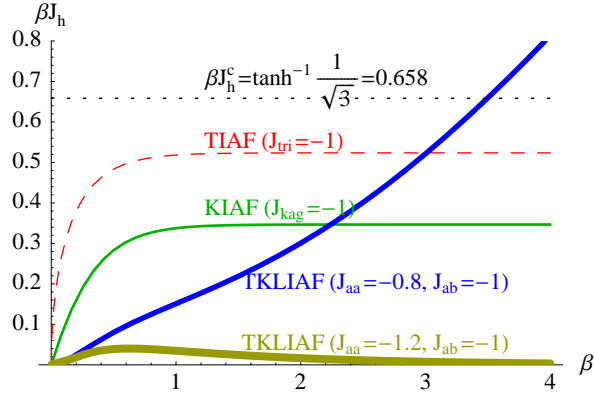


FIG. 3: (Color online). Effective dimensionless coupling  $\beta J_h$  of the honeycomb lattice Ising model as a function of the original inverse temperature  $\beta$ , for the triangular Ising antiferromagnet (TIAF), kagome Ising antiferromagnet (KIAF), or TKL Ising antiferromagnet (TKLIAF). In the case of the TIAF,  $\beta J_h$  is imaginary, and  $\text{Im } \beta J_h$  is shown as a dashed curve; for the KIAF and TKLIAF,  $\beta J_h$  is real. For the TKLIAF in the unfrustrated regime,  $\beta J_h$  crosses the dotted line (the critical coupling of the honeycomb Ising model), indicating a phase transition. The other models do not have phase transitions.

- For the triangular kagome lattice Ising antiferromagnet (TKLIAF) in the unfrustrated regime (e.g.,  $J_{aa} = -0.8, J_{ab} = -1$ ), the plot of  $\beta J_h$  intersects the dotted line, indicating a phase transition at  $\beta \approx 3.5$ .
- In contrast, for the TKLIAF in the frustrated regime ( $J_{aa} = -0.8, J_{ab} = -1$ ),  $\beta J_h$  grows to a maximum and then decays to zero, indicating the absence of a phase transition. Paradoxically, and unlike the other lattices, *stronger* bare couplings lead to a *weaker* effective coupling! The fact that  $\beta J_h \rightarrow 0$  as  $\beta \rightarrow \infty$  is closely connected to the fact that the residual entropy of the TKL lattice has the simple value of  $\ln 72$  per unit cell (as we will show), unlike the cases of the TIAF<sup>15</sup> and KIAF<sup>16</sup> in which the residual entropies are non-trivial two-dimensional integrals.

## B. Phase boundary

The phase boundary of the TKL Ising model in zero applied field was calculated in Ref. 11. We show an alternative exact derivation of the results here for pedagogical reasons. Once we have used the techniques of Sec. III A to map the TKL Ising model into the Ising model on a honeycomb lattice, we can use known results for the honeycomb lattice. The critical temperature of the honeycomb Ising model is given by  $t_h^c = \tanh \beta J_h = 1/\sqrt{3}$ , or, equivalently,  $x_h^c = \exp -2\beta J_h = 2 - \sqrt{3}$ . Substituting in the equivalent coupling of the honeycomb lattice, Eq. 17, leads to an implicit equation for the critical temperature

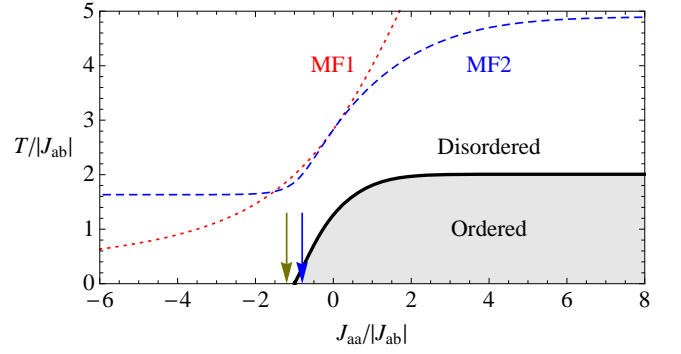


FIG. 4: (Color online) Phase diagram of the TKL Ising model in the  $(J_{aa}, T)$  plane, for  $J_{ab} = \pm 1$  and  $h = 0$ . The thick curve is the exact solution (equivalent to that in Ref. 11). The dotted and dashed curves are mean-field approximations (see Appendix, Sec. A). The ordered phase is ferromagnetic if  $J_{ab} > 0$  and ferrimagnetic if  $J_{ab} < 0$ . The disordered state is paramagnetic. For  $J_{aa} < -J_{ab}$ , it persists down to  $T = 0$ , where the entropy is  $\ln 72$  per unit cell and the susceptibility obeys a Curie law. The arrows indicate the two TKLIAF cases discussed in Fig. 3.

$1/\beta_c$  of the TKL Ising model:

$$e^{-4\beta_c J_{aa}} = (\sqrt{3} - 1) \cosh 4\beta_c J_{ab} - (\sqrt{3} + 1). \quad (18)$$

Eqn. 7 of Ref. 11 is equivalent to the simpler expression reported here. This critical curve is plotted in Fig. 4. For large ferromagnetic  $J_{aa}$ , the critical temperature saturates at a finite value,  $T_c/|J_{ab}| \approx 4/\ln(2 + \sqrt{3} + \sqrt{6 + 4\sqrt{3}}) \approx 2.00838$ . As  $J_{aa}$  is reduced towards  $-1$ , the critical temperature falls to zero. Near  $J_{aa} = -|J_{ab}|$ , the critical curve is approximately linear:

Since the mapping from the TKL to the honeycomb lattice preserves the nature of the singularity in the partition function, the phase transition is a continuous second-order transition in the 2D Ising universality class.

In zero field ( $h = 0$ ) the partition function  $Z$  is invariant under a change of sign of  $J_{ab}$ , and the topology of the phase diagram is independent of this sign, although the identification of the phases is not. First consider the model for the case  $J_{aa} = 0$ , where the TKL reduces to a decorated kagome lattice. If  $J_{ab}$  is ferromagnetic, the model develops *ferromagnetic* order below the Curie temperature. If  $J_{ab}$  is antiferromagnetic, the model develops *ferrimagnetic* order below the ordering temperature. Although the decorated kagome lattice is bipartite, the numbers of spins on the  $a$ - and  $b$ -sublattices are not equal: there are twice as many  $a$ -spins as  $b$ -spins. Hence we have *ferrimagnetic* order, with unequal numbers of up and down spins producing a net moment. However, the transition temperature, free energy, internal energy, specific heat, and entropy are independent of the sign of  $J_{ab}$  in the absence of applied field. Now introduce the coupling  $J_{aa}$ . If this is ferromagnetic, it has very little

effect, since the  $a$ -spins already have a tendency to align. However, if  $J_{aa}$  is antiferromagnetic, it fights against the ordering induced by  $J_{ab}$ . If  $J_{aa}$  is sufficiently antiferromagnetic, ( $J_{aa}/|J_{ab}| < -1$ ), the system is in a frustrated regime with no order even at zero temperature.

### C. Partition function

The partition function per unit cell,  $z_{\text{TKL}}$ , of the TKL Ising model is equal to that of the equivalent honeycomb lattice  $z_H$ , multiplied by the factors  $z_1, \dots, z_6$  below which are accumulated during the sequence of  $\nabla$ - $Y$  transformations and series reductions necessary to effect the transformation. These factors are

$$z_1 = \frac{1}{1 + x_4 x_3^2} \sqrt{\frac{x_4 x_3^2}{x_{aa} x_{ab}^2}} \quad (\text{first } \nabla - Y) \quad (19)$$

$$z_2 = (1 + x_3^2) \sqrt{\frac{x_5}{x_3^2}} \quad (J_3 \text{ in series}) \quad (20)$$

$$z_3 = (1 + x_4^2) \sqrt{\frac{x_6}{x_4^2}} \quad (J_4 \text{ in series}) \quad (21)$$

$$z_4 = \frac{1}{1 + x_7^3} \sqrt{\frac{x_7^3}{x_5^3}} \quad (\text{second } \nabla - Y) \quad (22)$$

$$z_5 = \frac{1}{1 + x_6 x_7} \sqrt{\frac{x_8}{x_6 x_7}} \quad (J_6, J_7 \text{ in series}) \quad (23)$$

$$z_6 = \frac{1}{1 + x_8 x_7} \sqrt{\frac{x_9}{x_8 x_7}} \quad (J_8, J_7 \text{ in series}) \quad (24)$$

The total accumulated partition function change is therefore

$$\begin{aligned} z_{\text{TKL}} &= z_1^6 z_2^6 z_3^3 z_4^2 z_5^3 z_6^3 z_H \\ &= \frac{(1 + x_{ab}^2)^2 (1 + 6x_{aa}^2 x_{ab}^2 + x_{ab}^4)^3}{1 + 2(1 + 6x_{aa}^2) x_{ab}^2 + x_{ab}^4} z_H. \end{aligned} \quad (25)$$

The partition function per unit cell of the honeycomb lattice has been calculated in the literature by, *e.g.*, the Pfaffian method<sup>17,18</sup>. It is

$$z_H(x_h) = \frac{\sqrt{2}(1 - x_h^2)}{x_h} \exp \left[ \frac{1}{2} \Omega(w(x_h)) \right] \quad (26)$$

where

$$\Omega(w) = \int_0^{2\pi} \frac{dp}{2\pi} \int_0^{2\pi} \frac{dq}{2\pi} \ln(w - \cos p - \cos q - \cos(p + q)) \quad (27)$$

and

$$w(x_h) = \frac{1 - 2x_h + 6x_h^2 - 2x_h^3 + x_h^4}{2x_h(1 - x_h)^2}. \quad (28)$$

For the purposes of numerical evaluation, we rewrite the function  $\Omega(w)$  in the following form

$$\Omega(w) = \frac{2}{\pi} \int_0^{\pi/2} dp \ln \left[ \cos p + \operatorname{arccosh} \frac{w - \cos 2p}{2 \cos p} \right]. \quad (29)$$

In order to get accurate numerical results one has to further split the range of integration according to the singularities of the integrand.

Thus the partition function of the TKL Ising model (per unit cell) is

$$z_{\text{TKL}}(x_{aa}, x_{ab}) = \Psi(x_{aa}, x_{ab}) \exp \left[ \frac{1}{2} \Omega(w(x_h(x_{aa}, x_{ab}))) \right] \quad (30)$$

where

$$\Psi = 2x_{aa}^{-3} x_{ab}^{-5} (1 - x_{ab}^4)^2 \times \sqrt{(1 + 3x_{aa}^2)(1 + 6x_{aa}^2 x_{ab}^2 + x_{ab}^4)} \quad (31)$$

and  $\Omega$ ,  $w$ , and  $x_h$  are defined in Eqs. ((27)), ((28)), ((17)), respectively. The total partition function  $Z_{\text{TKL}}$  is related to the partition function per unit cell  $z_{\text{TKL}}$  by  $Z_{\text{TKL}} \equiv z_{\text{TKL}}^N$ , where  $N$  is the number of unit cells. We show plots of  $-\ln z_{\text{TKL}}/(\beta|J_{aa}|)$  in Figs. 5 and 6 (red curves) in the unfrustrated and frustrated regimes, respectively.

### D. Energy

The energy per unit cell of the TKL Ising model can be obtained by differentiation of the partition function:

$$u = -\frac{d \ln z}{d\beta} = -\frac{dx_{aa}}{d\beta} \frac{\partial \ln z}{\partial x_{aa}} - \frac{dx_{ab}}{d\beta} \frac{\partial \ln z}{\partial x_{ab}} \quad (32)$$

$$= \sum_{i=aa,ab} J_i x_i \left[ 2 \frac{\partial \ln \Psi}{\partial x_i} + \frac{\partial x_h}{\partial x_i} \frac{dw}{dx_h} \frac{d\Omega}{dw} \right], \quad (33)$$

where  $\Psi$  is given in Eqn. 31.  $\frac{d\Omega}{dw}$  is the Green function of a particle on a triangular lattice and can be expressed in terms of the complete elliptic integral of the first kind,  $K$ :<sup>19</sup>

$$\frac{d\Omega}{dw} = \int_0^{2\pi} \frac{dp}{2\pi} \int_0^{2\pi} \frac{dq}{2\pi} \frac{1}{w - \cos p - \cos q - \cos(p + q)} \quad (34)$$

$$= -\frac{2}{\pi(-w-1)^{3/4}(-w+3)^{1/4}} \times \quad (35)$$

$$K \left( \frac{1}{2} + \frac{w^2 - 3}{2(w+1)(-w-1)^{1/2}(-w+3)^{1/2}} \right). \quad (36)$$

We show plots of  $-u/|J_{aa}|$  in Figs. 5 and 6 (green curves).

### E. Specific heat

The heat capacity per unit cell,  $c = \frac{du}{dT}$ , can be obtained by further differentiation:



$$\begin{aligned}
c = 2 & \left\{ (\beta J_{aa})^2 x_{aa} \left[ \frac{\partial^2 \ln \Psi}{\partial x_{aa} \partial x_{aa}} + \left( \frac{\partial x_h}{\partial x_{aa}} + \frac{\partial^2 x_h}{\partial x_{aa}^2} x_{aa} \right) w' \Omega' + \left( \frac{\partial x_h}{\partial x_{aa}} \right)^2 x_{aa} (w'' \Omega' + (w')^2 \Omega'') \right] \right. \\
& + [\text{previous term with } aa \text{ replaced by } ab] \\
& \left. + 2\beta^2 J_{aa} J_{ab} x_{aa} x_{ab} \left[ \frac{\partial^2 \ln \Psi}{\partial x_{aa} \partial x_{ab}} + \frac{\partial^2 x_h}{\partial x_{aa} \partial x_{ab}} w' \Omega' + \frac{\partial x_h}{\partial x_{aa}} \frac{\partial x_h}{\partial x_{ab}} (w'' \Omega' + (w')^2 \Omega'') \right] \right\} \quad (37)
\end{aligned}$$

where  $w'$ ,  $\Omega'$ , etc., represent derivatives of the functions  $w(x_h)$  and  $\Omega(w)$  with respect to their arguments. We show plots of  $c$  in Figs. 5 and 6 (blue curves).

In the unfrustrated case ( $J_{aa} > 0$ , Fig. 5), the specific heat has a broad hump just above  $T = J_{aa}$ , and a sharp peak near  $T = 2|J_{ab}|$ . The broad hump is due to ferromagnetic alignment within each  $a$ -plaquette. The sharp peak corresponds to the phase transition to a ferromagnetic (for  $J_{ab} > 0$ ) or ferrimagnetic (for  $J_{ab} < 0$ ) state, governed by the weakest links,  $J_{ab}$ . The position of the sharp peak is consistent with the solution of Eqn. 18. (See also Fig. 4.) In the frustrated case, broadened features remain at both of these energy scales, as shown in Fig. 6.

### F. Zero-temperature limit: residual entropy

Far from the critical curve, results for two limits can be obtained, corresponding to the ordered phase and to the disordered phase (which persists even at zero temperature).

In the first case,  $J_{aa}/|J_{ab}| > -1$ , the system orders at low temperatures, going into either the ferromagnetic state (for  $J_{ab} > 0$ ) or ferrimagnetic state (for  $J_{ab} < 0$ ). In the low temperature limit, the partition function and internal energy may be expanded as

$$\ln Z(\beta) = 6 \ln x_{ab} - 3 \ln x_{aa} + \frac{6x_{aa}^2}{x_{ab}^2} + \dots, \quad (38)$$

$$u(\beta) = -12|J_{ab}| + 6|J_{aa}| + 24e^{-4\beta|J_{ab}-J_{aa}|}|J_{ab} - J_{aa}| + \dots \quad (39)$$

As  $T \rightarrow 0$ , the residual entropy is zero, whether in the ferromagnetic phase or the ferrimagnetic phase.

Suppose  $J_{aa}/|J_{ab}| < -1$ . In this case, the model becomes frustrated when  $T \rightarrow 0$ ,  $\beta \rightarrow \infty$ . We have  $x_{aa}, x_{ab} \rightarrow \infty$ ,  $x_h \rightarrow 1^-$ ,  $w \rightarrow \infty$ . Expanding  $\Omega(w) \approx \ln w$  in a series in  $w$ , and then expanding  $\ln Z$  as a series in  $x_{aa}$  and  $x_{ab}$ , we find:

$$\begin{aligned}
\ln Z(\beta) = \ln 72 + \ln x_{aa} + 2 \ln x_{ab} \\
+ \frac{2}{x_{ab}^2} + \frac{1}{3x_{aa}^2} + \frac{x_{ab}^2}{6x_{aa}^2} + \dots \quad (40)
\end{aligned}$$

We can thus obtain the following low-temperature ap-

proximation for the energy per unit cell:

$$\begin{aligned}
u(\beta) = & -2|J_{aa}| - 4|J_{ab}| + \frac{2}{3}e^{-4\beta|J_{aa}-J_{ab}|}|J_{aa} - J_{ab}| \\
& + \frac{2}{3}e^{-4\beta|J_{aa}+J_{ab}|}|J_{aa} + J_{ab}| + \frac{4}{3}e^{-4\beta|J_{aa}|}|J_{aa}| \\
& + 8e^{-4\beta|J_{ab}|}|J_{ab}| + \dots \quad (41)
\end{aligned}$$

The first two terms are the ground state energy. The other terms represent different types of excitations about the ground state(s). The coefficients represent relative degeneracies of excited states and ground states, and the exponents represent excitation energies.

The first term in the series expansion of  $\ln Z$  gives the residual entropy per unit cell:

$$s_0 = \lim_{\beta J_{ab} \rightarrow -\infty} \lim_{\beta J_{aa} \rightarrow -\infty} (\ln Z + \beta u) = \ln 72. \quad (42)$$

Thus the residual entropy is exactly  $\ln 72 \approx 4.2767 \dots$  per unit cell, or  $\frac{1}{9} \ln 72 \approx 0.4752 \dots$  per site. This number will be discussed in more detail in Sec. IV.

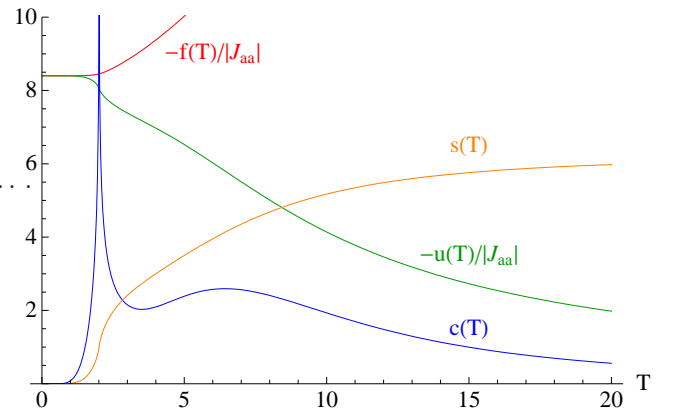


FIG. 5: (Color online). Thermodynamic functions vs temperature  $T$  for unfrustrated (ferromagnetic) couplings  $J_{aa} = 5$  and  $|J_{ab}| = 1$ . Red: free energy  $f(T) = -k_B T \ln Z$ . Green: energy  $u(T)$ . Blue: heat capacity  $c(T)$ . Yellow: entropy  $s(T)$ . All values quoted per unit cell; each unit cell contains 9 sites.

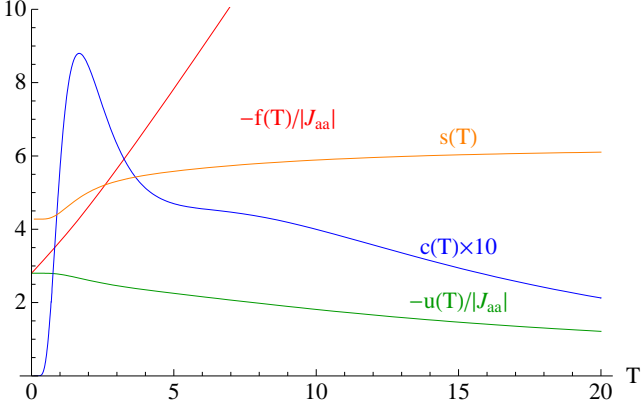


FIG. 6: (Color online). Thermodynamic functions vs temperature  $T$  in frustrated regime,  $J_{aa} = -5$  and  $|J_{ab}| = 1$ , where the intratrimer coupling  $J_{aa}$  is strong and antiferromagnetic.

#### IV. EXACT RESULTS AT ZERO TEMPERATURE

In this section we show how the zero-temperature phase diagram (along with the thermodynamic properties and correlations of the various phases) can be systematically deduced with and without applied field by considering ground states of large triangular plaquettes. By explicitly comparing the ground state energies, we derive the phase diagram. The results of this section are summarized in Figs. 10 and 11.

##### A. Zero Field (phases V and VI)

The phase diagram for zero applied field is shown in Fig. 4. For  $J_{aa} > -|J_{ab}|$  and low temperature, the system is in an ordered phase which is ferromagnetic for  $J_{ab} > 0$ , and ferrimagnetic if  $J_{ab} < 0$ . For  $J_{aa} < -|J_{ab}|$ , the system remains disordered even at zero temperature, with a residual entropy of  $s_0 = \ln 72$ . The zero-field disordered phase is labeled phase V in Figs. 10 and 11, and the zero-field ordered phase is labeled phase VI.

The degeneracy of the ground state manifold can be understood by considering the energetics of a single large plaquette, *i.e.*, an  $a$ -spin trimer along with its enclosing  $b$ -spin trimer. Representative plaquette configurations within the ground state are shown in Fig. 7. We enumerate all possible plaquette energies in Table I. As can be seen from the table, for any of the  $2^3 = 8$  possible configurations of the  $b$ -trimer, there are three and only three configurations of the enclosed  $a$ -trimer which are all within the ground state.<sup>39</sup> This means that the  $b$ -spins are effectively free within the ground state manifold.

In order to count the ground state degeneracy, we now turn to the unit cell. Since the  $b$ -spins are free, and there are 3  $b$ -spins per unit cell, this contributes  $2^3 = 8$  configurations

per unit cell to the ground state manifold. For any given configuration of the  $b$ -spins, each  $a$ -trimer in the lattice has a 3-fold degeneracy. Since there are two  $a$ -trimers per unit cell, these contribute a factor of  $3^2 = 9$  to the ground state degeneracy. The total degeneracy per unit cell in the ground state is therefore  $8 \times 9 = 72$ , as we showed in Sec. III F.

The fact that the  $b$ -spins are effectively independent also means that the correlation function is “perfectly localized”: it is exactly zero beyond a distance  $r_{bb}$  (the distance between two  $b$ -spins). The correlation length  $\xi$  is thus zero (where  $\xi$  is defined as the asymptotic decay length of the correlation function at *large* distances).

For comparison, at  $T = h = 0$ , the triangular Ising AF has power-law correlations. The kagome Ising AF is more frustrated than the triangular lattice case, since its ground state has exponentially decaying correlations. We have shown here that the ground state of the TKL Ising AF in the frustrated regime has perfectly localized correlations, making this model even more frustrated than either the triangular or kagome cases.

		$\sigma_a$							
$\sigma_b$	$\uparrow\uparrow\uparrow$	$\uparrow\uparrow\uparrow$	$\uparrow\uparrow\downarrow$	$\uparrow\downarrow\uparrow$	$\uparrow\downarrow\downarrow$	$\downarrow\uparrow\uparrow$	$\downarrow\uparrow\downarrow$	$\downarrow\downarrow\uparrow$	$\downarrow\downarrow\downarrow$
	$\uparrow\uparrow\uparrow$	15	-1	-1	-1	<b>-5</b>	<b>-5</b>	<b>-5</b>	3
	$\uparrow\uparrow\downarrow$	11	<b>-5</b>	-1	-1	-1	<b>-5</b>	<b>-5</b>	7
	$\uparrow\downarrow\uparrow$	11	-1	<b>-5</b>	-1	<b>-5</b>	-1	<b>-5</b>	7
	$\uparrow\downarrow\downarrow$	11	-1	-1	<b>-5</b>	<b>-5</b>	<b>-5</b>	-1	7
	$\downarrow\uparrow\uparrow$	7	-1	<b>-5</b>	<b>-5</b>	<b>-5</b>	-1	-1	11
	$\downarrow\uparrow\downarrow$	7	<b>-5</b>	-1	<b>-5</b>	-1	<b>-5</b>	-1	11
	$\downarrow\downarrow\uparrow$	7	<b>-5</b>	<b>-5</b>	-1	-1	-1	<b>-5</b>	11
	$\downarrow\downarrow\downarrow$	3	<b>-5</b>	<b>-5</b>	<b>-5</b>	-1	-1	-1	15

TABLE I: Energy of a large triangle (consisting of 3  $b$ -spins and 3  $a$ -spins) as a function of the configurations of  $a$  and  $b$  spins. For clarity of presentation, we present the results for the case  $J_{aa} = -3$ ,  $J_{ab} = -1$ ,  $h = 0$ , but the form of the table is representative of the entire line  $J_{aa}/|J_{ab}| < -1$ . The boldfaced numbers indicate the lowest-energy configurations, which have energy  $J_{aa} + 2J_{ab}$ . Note that each row contains exactly three boldfaced numbers. See text for discussion.

##### B. Saturated ferromagnetic phase (phase I)

At very high fields, when  $h/|J_{ab}| > \max(4, 2|J_{aa}|/|J_{ab}| + 2)$ , we find that there is a unique ground state where all the  $b$ -spins and  $a$ -spins are up. This state is easily seen to have magnetization  $m = 9$ , entropy  $s = 0$ , and energy  $u = -3h + 6|J_{aa}| + 12|J_{ab}|$  per unit cell.

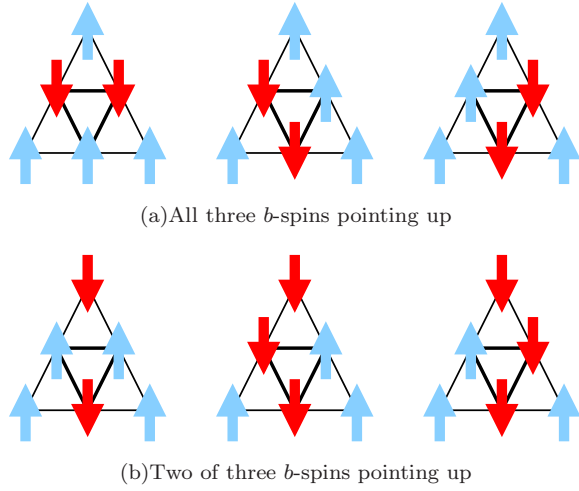


FIG. 7: (Color online). The  $\ln 72$  phase. Given a configuration of the three  $b$ -spins (on the outer triangle), it can be shown, by enumerating all possibilities, that there are exactly three states of the  $a$ -spins (on the inner triangle). The figure illustrates this for two configurations of  $b$ -spins; results for the other configurations can be seen from the Ising symmetry and the local rotational symmetry of the triangular plaquettes.

### C. Ferrimagnetic phase (phase II)

At lower fields  $0 < h/|J_{ab}| < 4$  and when  $J_{aa}/|J_{ab}| > -1$ , there is a ferrimagnetic phase: the  $a$ -spins, being more numerous, align parallel to the field (up); the  $b$ -spins are then induced to point down due to the antiferromagnetic  $J_{ab}$  interaction. This phase has  $m = 3$ ,  $s = 0$ , and  $u = -3h + 6|J_{aa}| - 12|J_{ab}|$  per unit cell.

### D. Log 9 phase (phase III)

If  $4 < h/|J_{ab}| < 2|J_{aa}|/|J_{ab}| + 2$ , the  $b$ -spins are completely polarized, but each  $a$ -triangle has 3 degenerate states (see Fig. 8). Therefore, in this phase the system is equivalent to a set of non-interacting three-state Potts spins. This phase has  $m = 5$ ,  $s = \ln 9 = 2.1972\dots$ , and  $u = -5h - 2|J_{aa}| + 4|J_{ab}|$  per unit cell. Again, the correlation function is perfectly localized, and the correlation length is  $\xi = 0$ .

### E. Dimer phase (phase IV)

The most interesting situation occurs when  $0 < h/|J_{ab}| < 4$  and  $J_{aa}/|J_{ab}| < -1$ . Table I shows that the system will have the lowest energy if each  $b$ -trimer has exactly one  $b$ -spin pointing down. Counting the number of ways to satisfy this constraint globally is a non-trivial problem. The situation is the same as that for a kagome Ising AF at  $T = 0$  and  $0 < h < 4|J_{\text{kagome}}|$ , which has been studied before<sup>20,21,22,23</sup>. The down- $b$ -spins behave

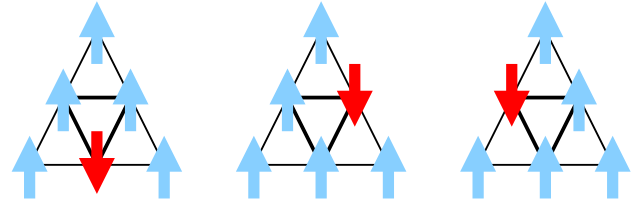


FIG. 8: (Color online). Phase III of the TKL Ising model. When the field is quite strong, the  $b$ -spins (outer triangle) are all polarized, and each  $a$ -trimer (inner triangle) has three degenerate ground states.

like a lattice gas on the kagome lattice with nearest-neighbor exclusion, at maximal density. The ground states can be mapped to configurations of dimers occupying a honeycomb lattice (see Fig. 9). This problem has been solved exactly using the Pfaffian method<sup>17</sup>; the entropy per unit cell is

$$\frac{1}{8\pi^2} \int_0^{2\pi} dp \int_0^{2\pi} dq \ln(1 - 4 \cos p \cos q + 4 \cos^2 q) = 0.3231\dots \quad (43)$$

Therefore, the entropy of the TKL phase IV is also  $0.3231\dots$  per unit cell, or  $0.03590\dots$  per site.

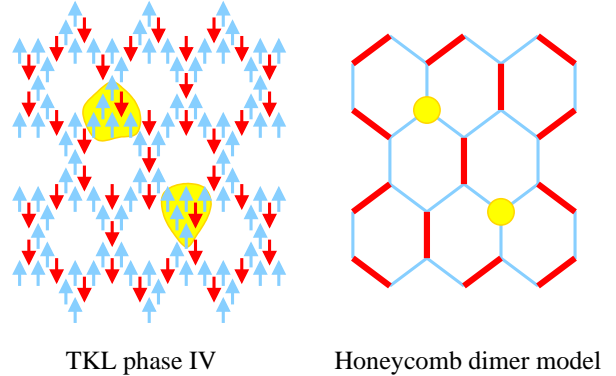


FIG. 9: (Color online). Phase IV of the TKL Ising model: Mapping of the spin configurations to configurations of dimers on a honeycomb lattice. The yellow patches represent defects in the spin configuration, which correspond to vacancies (or monomers) in the dimer picture.

The correlation function of the  $b$ -spins,  $C_{bb}(\mathbf{r}) = \langle \sigma_b(\mathbf{0}) \sigma_b(\mathbf{r}) \rangle$ , is equivalent to the dimer-dimer correlation function. This correlation function decays as a power law,  $1/r^2$ , and nice visualizations in real space and reciprocal space are given in Ref. 23. Thus, the model is in a critical phase, in the ‘‘Villain-Stephenson universality class’’. The magnetization per unit cell is  $m = 3$  and the energy per unit cell is  $u = -3h - 2|J_{aa}| - 4|J_{ab}|$ .



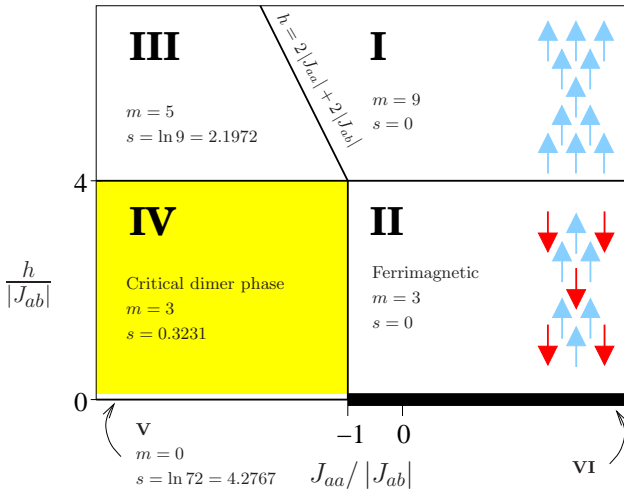


FIG. 10: (Color online). Phase diagram of the TKL Ising model in the  $(J_{aa}, h)$  plane, for  $J_{ab} < 0$  (antiferromagnetic intertrimer coupling) and  $T = 0$ . The phase diagram is symmetric under a change of sign of  $h$ . The phases I', II', III', IV' are just mirror images of I, II, III, IV obtained by swapping up and down spins. The yellow region represents the critical phases with power-law correlations; note that it does not include the thin line at  $h = 0$ , which is phase V, the  $\ln 72$  phase described in the text. The thick line (VI) persists as a true ferrimagnetic phase transition at finite  $T$ ; all other lines turn into crossovers.

## F. Phase diagram

We now combine the above results in order to report the full phase diagram of the TKL Ising model. Fig. 10 shows the phase diagram for antiferromagnetic intertrimer coupling,  $J_{ab} < 0$ , and in Fig. 11 we show the phase diagram for ferromagnetic intertrimer coupling,  $J_{ab} > 0$ . In both cases, the phase diagram is symmetric under for  $h \rightarrow -h$ , with simultaneous change of sign of all spins. The entropy and magnetization change discontinuously across every zero-temperature phase boundary. Exactly on the phase boundaries and intersections of these boundaries, the entropy will be higher than in either adjacent phase, because the system can choose from states within each set of ground states.

Note that the high-field phases (I and III) are common to both phase diagrams. The more interesting case is that of Fig. 10, which has antiferromagnetic intertrimer coupling  $J_{ab} < 0$ , and more phases at intermediate field strength. Right at  $h = 0$  in both phase diagrams, the ground state is phase V, the spin liquid with residual entropy  $s_0 = \ln 72$  that we discussed in Sec. IV A. When  $J_{ab} < 0$ , the application of an infinitesimal field induces a critical state with power law correlation functions (phase IV), which we have mapped to the problem of hard-core dimers on a honeycomb lattice.

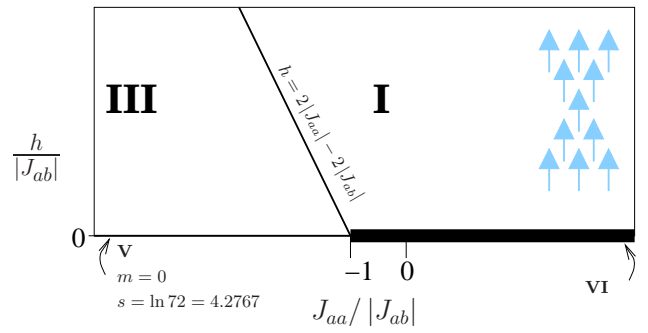


FIG. 11: (Color online). Phase diagram of the TKL Ising model in the  $(J_{aa}, h)$  plane, for  $J_{ab} > 0$  (ferromagnetic intertrimer coupling) and  $T = 0$ .

## V. FINITE TEMPERATURE AND FINITE FIELD

Most of the phase transitions in the zero-temperature phase diagrams are destroyed by thermal fluctuations. The clear exception is phase VI, which has spontaneously broken  $Z_2$  symmetry. This long-range ordered phase survives at finite temperature, and has a true phase transition at a Curie temperature  $T_c \neq 0$ . Since  $h$  is a relevant perturbation, this finite-temperature phase transition is destroyed at any finite field, leaving only a crossover.

The other transitions in Figs. 10 and 11 are not characterized by a *spontaneously* broken symmetry with an order parameter. Therefore, they cannot persist at finite  $T$  as traditional order-disorder transitions. However, a more subtle analysis is required to understand whether the critical phase, phase IV, persists at finite  $T$  (bounded, e.g., by a Kosterlitz-Thouless transition curve). The situation is quite similar to that for the kagome Ising AF described in Ref. 23. Based on the table of ground state energies, Table I, it is possible to enumerate the types of defects that can occur in phase IV. These defects correspond to breaking a dimer into two monomers (see Fig. 9), and can only be created in pairs. Each defect has energy  $\Delta U = \min(h, 4|J_{ab}| - h)$ . The entropy  $\Delta S$  associated with creating a defect pair is at least  $O(\ln L^2)$ , because one may choose to break any of the  $O(L^2)$  dimers; in fact the entropy is even greater than this because the resulting monomers can be moved apart, resulting in many new configurations. Hence at any finite  $T$ , the density of monomers is finite. A theorem of Lieb and Heilmann<sup>24</sup> states that monomer-dimer models cannot have phase transitions at any finite density of monomers. Therefore, *the critical phase only exists at  $T = 0$ , and it is destroyed at finite  $T$ .*

However, if the density of monomers is low, the correlation length  $\xi$  may still be long; naively, one might expect  $\xi^2 \sim 1/n_{\text{monomers}} \propto \exp(E_{\text{monomer}}/T)$ , but a more careful treatment accounting for the effective Coulomb attraction between monomers gives the result  $\xi^2 \sim 1/n_{\text{monomers}} \propto \exp(8E_{\text{monomer}}/7T)$ .<sup>23</sup> This scenario is consistent with the size-dependent peaks in the suscep-

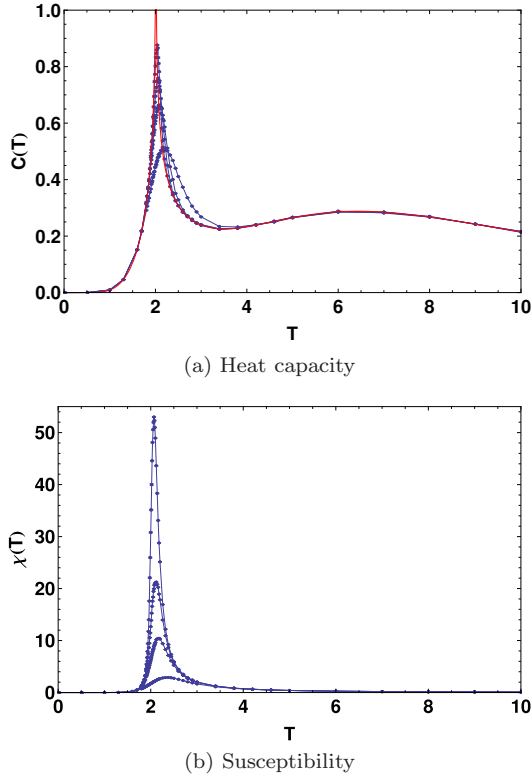


FIG. 12: (Color online). Temperature dependence of heat capacity and susceptibility from Monte Carlo simulation for  $J_{aa} = 5$  and  $J_{ab} = +1$  with system sizes  $L = 12, 24, 36, 60$ . Red line (no dots) represents the exact solution of specific heat. Peaks become taller and narrower as  $L$  increases.

tibility that we find from Monte Carlo simulations (see Sec. VI).

## VI. MONTE CARLO SIMULATIONS

In this section we present the results of Monte Carlo (MC) simulations of the TKL Ising model, Eq. (1), for various combinations of parameters. The simulations corroborate our analytic predictions and also allow us to perform calculations at finite  $h$  and  $T$  as well as to compute the magnetization and susceptibility.

We use the Wolff algorithm for  $J_{aa} > 0$  at  $h = 0$ , and the Metropolis algorithm for  $J_{aa} < 0$  at  $h = 0$  and  $h \neq 0$ . The system sizes we use are  $L = 12, 24, 36, 60$ , where  $L$  is the length of the underlying triangular lattice, so that the total number of spins is  $N = \frac{9}{16}L^2$ ; for periodic boundary conditions,  $L$  should be a multiple of 3 in order to avoid introducing boundary defects and additional frustration.

In order to evaluate the heat capacity  $C$  and magnetic susceptibility  $\chi$ , we use the fluctuation-dissipation theo-

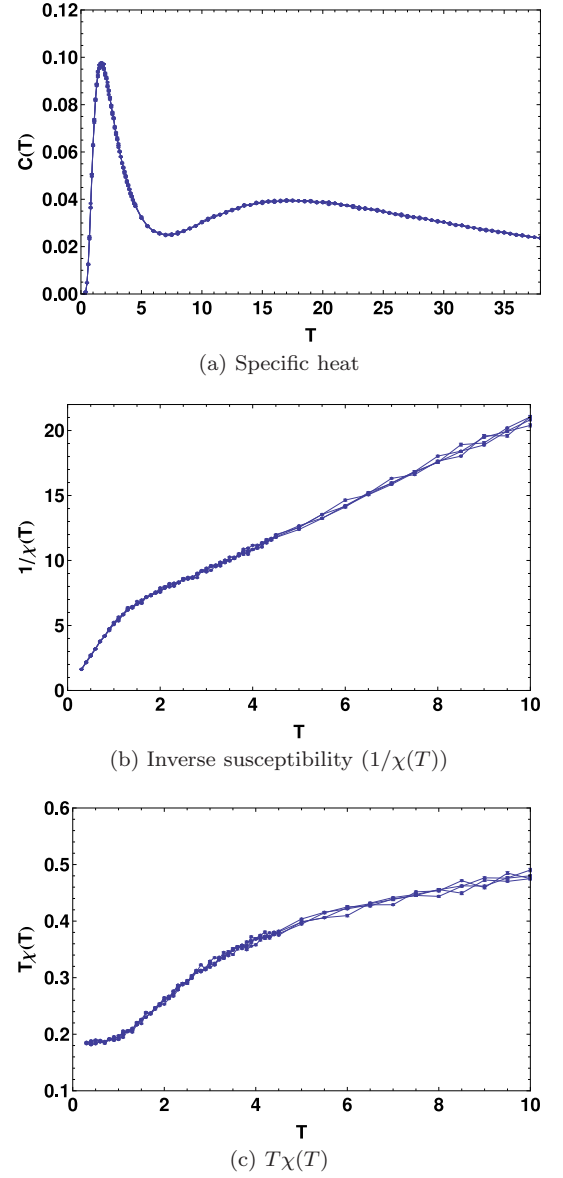


FIG. 13: (Color online). Temperature dependence of heat capacity and inverse susceptibility ( $1/\chi(T)$ ) and  $T\chi(T)$  from Monte Carlo simulation for  $J_{aa} = -10$  and  $J_{ab} = -1$  with system sizes  $L = 12, 24, 36, 60$ .

rem:

$$C = \frac{\langle H^2 \rangle - \langle H \rangle^2}{NT^2}, \quad (44)$$

$$\chi = \frac{\langle M^2 \rangle - \langle M \rangle^2}{NT}, \quad (45)$$

where  $\langle H \rangle$  and  $\langle M \rangle$  are the Monte Carlo averages of the total energy (i.e., the Hamiltonian) and magnetization, respectively. We define the sublattice magnetizations as

$$m_a = \frac{1}{N_a} \sum_{i \in a} \sigma_{ai}, \quad (46)$$

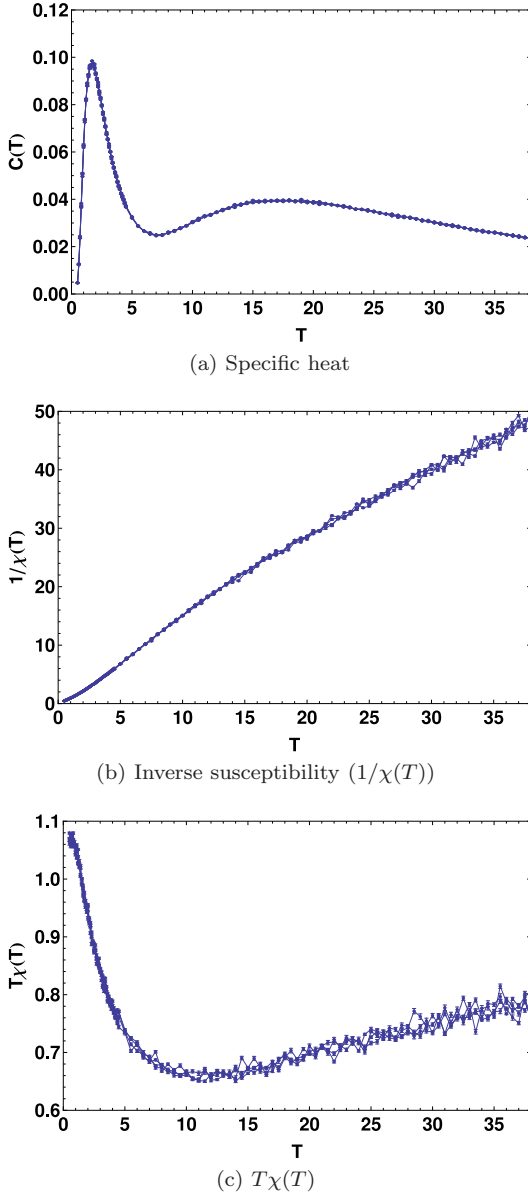


FIG. 14: (Color online). Temperature dependence of heat capacity, inverse susceptibility ( $1/\chi(T)$ ) and  $T\chi(T)$  from Monte Carlo simulation for  $J_{aa} = -10$  and  $J_{ab} = 1$  with system sizes  $L = 12, 24, 36, 60$ .

$$m_b = \frac{1}{N_b} \sum_{i \in b} \sigma_{bi} , \quad (47)$$

where  $N_a$  is the number of  $a$ -spin sites, and  $N_b$  is the number of  $b$ -spin sites.

### A. Zero magnetic field

We first show Monte Carlo results at zero field. Fig. 12 shows the temperature evolution of the heat capacity and susceptibility in a representative unfrustrated case,  $J_{aa} = 5J_{ab} > 0$ . The Monte Carlo results for the heat capacity

are consistent with the exact results in Sec. IV; the peak in the heat capacity in our simulations becomes taller and narrower as  $L$  increases, tending towards the exact solution for  $L = \infty$ .

Figs. 13 and 14 show results for two frustrated parameter combinations ( $J_{aa}/|J_{ab}| < -1$ ). In both cases, the susceptibility shows a marked difference from the case of ferromagnetic intratrimer coupling,  $J_{aa} > 0$ . For  $J_{aa} > 0$ , the susceptibility shows a sharp peak at the Curie temperature  $T_c$ , whereas for  $J_{aa} < 0$ , it tends to  $\infty$  as  $T \rightarrow 0$ .

Unlike the free energy, heat capacity, entropy, and internal energy, the susceptibility depends on the sign of  $J_{ab}$ . Our predictions about the susceptibility can be used to distinguish whether a physical TKL Ising system has ferromagnetic or antiferromagnetic coupling between the  $a$  and  $b$  sublattices. For  $J_{ab} > 0$ , the inverse susceptibility  $1/\chi(T)$  shows two linear pieces, with a crossover at the lower coupling constant  $J_{ab}$ . However, when  $J_{ab} < 0$ , the inverse susceptibility approaches zero much slower than the  $J_{ab} > 0$  case.

The difference between antiferromagnetic and ferromagnetic coupling  $J_{ab}$  is even more evident in the plots of  $T\chi$ . At low temperatures,  $T\chi$  tends to a small finite constant as  $T \rightarrow 0$  if the intertrimer coupling is antiferromagnetic,  $J_{ab} < 0$ ; whereas, if the intertrimer coupling is ferromagnetic,  $J_{ab} > 0$ ,  $T\chi$  goes through a minimum around  $T \sim J_{aa}$ , increases sharply, and saturates at a finite value as  $T \rightarrow 0$ .

### B. Finite magnetic field

In Figs. 15 and 16, we show Monte Carlo results at finite field  $h$  and low temperature  $T = 0.1$  for  $J_{aa} = -2$  and  $J_{ab} = -1$ . The magnetization curves in Fig. 15 have a series of steps and plateaux (as is typical of frustrated spin systems). Starting from  $h = 0$ , as a field is applied, both the  $a$  and  $b$  sublattices immediately respond as the critical dimer phase is induced, developing (normalized) sublattice magnetizations of  $m_a = m_b = 1/3$ . As field is increased, the  $b$ -spins are more easily polarized, while the  $a$ -sublattice spins only become fully polarized when the magnetic field is strong enough.

The susceptibility as a function of applied field has a series of peaks, as shown in Fig. 16. The peaks at  $h = \pm 4$  increase with increasing system size from  $L = 12$  to  $L = 24$ . This indicates that the correlation length (in the vicinity of the peaks) is comparable to, or larger than, the system size. This does not indicate a true finite-temperature phase transition. Rather, because phase IV is critical (with infinite correlation length), the correlation length diverges as temperature is lowered toward this phase. At the low temperatures we have simulated, the correlation length is comparable to our system sizes. See Sec. V.

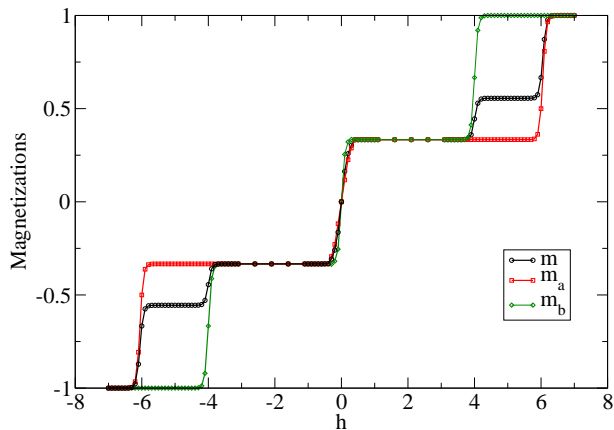


FIG. 15: (Color online). Magnetization  $m$  vs. external field  $h$  from Monte Carlo simulation for  $J_{aa} = -2$ ,  $J_{ab} = -1$  at  $T = 0.1$  for  $L = 12$ . Sublattice magnetizations  $m_a$  and  $m_b$  are also shown.

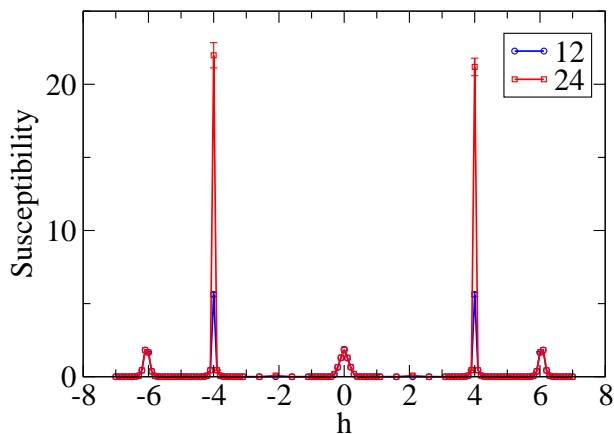


FIG. 16: (Color online). Susceptibility  $\chi$  vs. external field  $h$  from Monte Carlo simulation for  $J_{aa} = -2$ ,  $J_{ab} = -1$  at  $T = 0.1$  for  $L = 12$ .

## VII. DISCUSSION

Phases I, II, and III can easily be simulated using the Metropolis algorithm. However, phase IV has extremely slow dynamics when simulated using the Metropolis algorithm at low temperature – this could be described as glassy dynamics. We believe that the simulations may be made more efficient by using geometric cluster methods<sup>25</sup> or by augmenting the Metropolis algorithm with directed-loop updates tailored to the honeycomb dimer state.<sup>26,27</sup> The slow dynamics under the Metropolis algorithm may, however, be representative of the true dynamics in a physical realization of the TKL Ising antiferromagnet.

It may be possible to stabilize more phases at finite temperature by introducing an appropriate perturbation. For example, introducing coupling in the third direction may be sufficient to stabilize the critical phase at finite  $T$ . In addition, it may be possible to induce a Kasteleyn

transition in phase IV by applying some kind of orienting field (*e.g.*, uniaxial strain) to the TKL, similar to what was suggested by Moessner and Sondhi<sup>23</sup> on the Kagome lattice. In light of existing studies on triangular and kagome lattices, it is reasonable to expect that adding next-nearest-neighbor interactions to the TKL will produce an even richer phase diagram, like Kagome lattice.<sup>28</sup>

### A. Comparison with Other Frustrated Ising Models

In Table II, we present a comparison of the spin-spin correlations and the residual entropy among the frustrated TKL, triangular, and kagome lattices. The simplest example of a geometrically frustrated system is the triangular Ising antiferromagnet (TIAF), *i.e.*, a set of Ising spins on a triangular lattice with antiferromagnetic pairwise couplings. Due to the presence of odd cycles in the lattice graph, it is impossible for all pairs of nearest neighbor spins to be simultaneously antiparallel. As a result, the antiferromagnetic interactions are unable to produce long-range order even at zero temperature. Instead, at zero temperature, the TIAF has a quasi-long-range-ordered state in which the correlations decay with distance as  $r^{-1/2}$ .<sup>29,30</sup> This ground state is macroscopically degenerate, with a zero-temperature residual entropy of  $0.3231k_B$  per spin.<sup>15,31,32,33</sup> This number is the same as the entropy per unit cell of the random dimer model on a honeycomb lattice, and it crops up in many other places. Although the TIAF has no phase transition in zero field, the application of a finite field produces a surprisingly rich phase diagram. A small field induces a Berezinskii-Kosterlitz-Thouless (BKT) transition to a ‘spin crystal’ phase that breaks translational symmetry and has long-range order – the correlation function oscillates with distance but does not decay. At larger fields the crystalline order is destroyed via a transition in the 3-state Potts universality class. In this limit the TIAF is related to Baxter’s exactly soluble hard hexagon lattice gas model.<sup>34</sup>

Another frustrated spin system is the antiferromagnetic Ising model on a kagome lattice, formed by periodic removal of a quarter of the sites from the triangular lattice. Unlike the TIAF, the KIAF in the absence of field has pair correlations that decay exponentially at all temperatures including  $T = 0$ .<sup>35,36</sup> Its ground state entropy is  $1.5055k_B$  per unit cell or  $0.5018k_B$  per spin,<sup>16</sup> higher than that of the TIAF because the smaller coordination number allows more freedom. At finite  $h$ , there is a different spin liquid state that can be mapped to random dimers on a honeycomb lattice. In this state the spin-spin correlation function decays as a power law,  $1/r^2$ . The residual entropy is  $0.3231k_B$  per unit cell, or  $0.1077k_B$  per spin.

The ground state of the TKL Ising AF without applied field is even more frustrated than that of the kagome lattice: the correlation function becomes exactly zero be-

Lattice	Entropy	Spin-spin correlation
Triangular	0.3231...	$r^{-1/2}$
Triangular in field	0	long-range-ordered
Kagome	1.5055...	$e^{-r/\xi}$
Kagome in weak field	0.3231...	$r^{-2}$
TKL	$\ln 72$	0 for $r \geq r_{bb}$
TKL in weak field	0.3231...	$r^{-2}$
TKL in medium field	$\ln 9$	0 for $r \geq r_{bb}$

TABLE II: Comparison of various frustrated Ising models at  $T = 0$ . Residual entropies are quoted per unit cell; they are the logarithms of irrational numbers, unless otherwise stated.

yond a certain cutoff radius. The residual entropy per spin is  $\frac{1}{9} \ln 72 = 0.4752\dots$ . At finite  $h$ , there is a correlated, critical spin liquid state which we have mapped to hard core dimers on a honeycomb lattice. This state has a residual entropy of  $0.3231k_B$  per unit cell, or  $0.03590$  per spin. (See Table II.)

## B. Comparison with Experiment

As discussed in the introduction, the recently fabricated family of compounds  $\text{Cu}_9\text{X}_2(\text{cpa})_6 \cdot x\text{H}_2\text{O}$  have an arrangement of the copper sites which forms a triangular kagome lattice. There is no evidence of spontaneous magnetization down to at least  $T = 1.7\text{K}$ ,<sup>7</sup> consistent with a spin liquid ground state, which indicates that  $J_{aa}$  is antiferromagnetic. However, there is no agreement yet as to whether  $J_{ab}$  is ferromagnetic or antiferromagnetic.<sup>7,9</sup>

In studying the magnetic susceptibility, several groups find that the slope of  $1/\chi$  versus  $T$  is roughly linear at high temperature, but as  $T$  is lowered, the slope increases.<sup>7,8,37</sup> This is consistent with either  $J_{ab}$  ferromagnetic or antiferromagnetic, as seen in Figs. 13(b) and 14(b). A distinction can be made, though, by the behavior of  $T\chi$ . Whereas  $T\chi$  saturates to a finite value at low  $T$  for antiferromagnetic intertrimer coupling  $J_{ab} < 0$ ,  $T\chi$  reaches a minimum at intermediate  $T$  before saturating at a finite value as  $T \rightarrow 0$  if the intertrimer coupling is *ferromagnetic*,  $J_{ab} > 0$ . To the extent that the  $\text{Cu}_9\text{X}_2(\text{cpa})_6 \cdot x\text{H}_2\text{O}$  materials can be described by an Ising TKL model like the one in this paper, our calculations indicate that the intertrimer coupling must be ferromagnetic,  $J_{ab} > 0$ , so that upon application of a field, the system should be in Phase III, rather than Phase IV. Since there is a striking difference in the residual entropies in these two phases ( $s_0 = \ln 9 = 2.1972\dots$  in Phase III *vs.*  $s_0 = 0.3231\dots$  in Phase IV), heat capacity measurements will also be useful in distinguishing these phases. Other future experiments, including neutron scattering, NMR, and  $\mu\text{SR}$ , can also provide useful data for comparing to models of frustrated magnetism on the TKL.

## VIII. CONCLUSIONS

In conclusion, we have studied an Ising model on the triangular kagome lattice (TKL) with two interactions  $J_{aa}$  and  $J_{ab}$ , temperature  $T$ , and external field  $h$ . We have calculated the complete phase diagram in  $(J_{aa}, J_{ab}, h, T)$  parameter space *exactly*. Furthermore, we have obtained exact results for thermodynamic quantities (free energy, energy, heat capacity, and entropy) at all  $T$  for  $h = 0$ , and at all  $h$  for  $T = 0$ , and plotted them for representative cases.

In the experimentally relevant regime,  $|J_{aa}| \gg |J_{ab}|$ , if  $J_{aa}$  is ferromagnetic, the specific heat shows a broad hump corresponding to intra-trimer ordering, as well as a sharp peak at lower temperatures due to the onset of true long-range order. If  $J_{aa}$  is antiferromagnetic there are two broad features.

We have computed the magnetization  $M(T, h)$  and susceptibility  $\chi(T, h)$  in various regimes using Monte Carlo simulations. To the extent that experiments on the  $\text{Cu}_9\text{X}_2(\text{cpa})_6 \cdot x\text{H}_2\text{O}$  materials can be compared with an Ising TKL model, our calculations indicate that  $J_{ab} > 0$ .

We find that at strong frustration and zero field, as temperature is reduced, the model enters a spin liquid phase with residual entropy  $s_0 = \ln 72$  per unit cell, with “perfectly localized” correlations. This stands in contrast with the triangular and kagome Ising antiferromagnets, whose residual entropies cannot be expressed in closed form.

The most interesting feature of the model is a correlated critical spin liquid phase (with power-law correlations) that appears at strong frustration, weak fields, and zero temperature. We have mapped this phase to hard core dimer coverings of a honeycomb lattice. The critical power-law correlations are reduced to exponential correlations at finite  $T$ , but the correlation length may still be large. Such a phenomenon would be detectable by neutron scattering measurements.

## Acknowledgments

It is a pleasure to thank T. Takagi, M. Mekata, G. Ortiz, N. Sandler, and M. Ma for helpful discussions. This work was supported by Purdue University and Research Corporation (Y. L. L. and D. X. Y.). E. W. C. is a Cottrell Scholar of Research Corporation.

## APPENDIX A: MEAN-FIELD APPROXIMATIONS

For pedagogical purposes, we examine the zero-field TKL Ising model using two mean-field approaches. Compared with the exact solution (see Fig. 4), we see that such approaches can be quite misleading in the frustrated regime  $J_{aa}/|J_{ab}| < -1$ .



In the simplest mean-field approximation (MF1), every spin is assumed to fluctuate thermally in a mean field determined by the average magnetizations of its neighbors. This leads to a pair of simultaneous equations for the spontaneous magnetizations of the  $a$ - and  $b$ -sublattices,  $m_a = \langle \sigma_a \rangle$  and  $m_b = \langle \sigma_b \rangle$ ,

$$\begin{aligned} m_a &= \tanh \beta (2J_{aa}m_a + 2J_{ab}m_b), \\ m_b &= \tanh \beta (4J_{ab}m_a). \end{aligned} \quad (\text{A1})$$

where  $\beta = 1/T$ . Linearizing the tanh function in  $\langle \sigma_a \rangle$  and  $\langle \sigma_b \rangle$  gives the critical temperature,

$$T_c^{\text{MF1}} = J_{aa} + \sqrt{J_{aa}^2 + 8J_{ab}^2}. \quad (\text{A2})$$

We also present a more advanced mean-field approximation (MF2), similar to the method used by Strečka<sup>9</sup> for the quantum Heisenberg TKL model, in which we sum over all eight states of the  $a$ -trimers with appropriate Boltzmann weights instead of treating each  $a$ -spin independently. The mean-field equations are then

$$\begin{aligned} m_a &= \frac{e^{4\beta J_{aa}} \sinh 6\beta J_{ab}m_b + \sinh 2\beta J_{ab}m_b}{e^{4\beta J_{aa}} \cosh 6\beta J_{ab}m_b + 3 \cosh 2\beta J_{ab}m_b}, \\ m_b &= \tanh \beta (4J_{ab}m_a), \end{aligned} \quad (\text{A3})$$

and the critical temperature is given by

$$\frac{T_c^{\text{MF2}}}{|J_{ab}|} = \sqrt{\frac{8(1 + 3e^{4J_{aa}/T_c^{\text{MF2}}})}{(3 + e^{4J_{aa}/T_c^{\text{MF2}}})}}. \quad (\text{A4})$$

$T_c^{\text{MF1}}$  and  $T_c^{\text{MF2}}$  are the dotted and dashed curves, respectively, in Fig. 4. The mean-field approximations overestimate  $T_c$  by a factor of two or more. In the regime  $J_{aa}/|J_{ab}| \gg 1$ ,  $T_c$  is dominated by the weak links ( $J_{ab}$ ), so  $T_c/|J_{ab}|$  tends to a constant, a fact which is captured by MF2. However, in the frustrated regime  $J_{aa}/|J_{ab}| < -1$ , both MF1 and MF2 predict the wrong behavior of  $T_c$  (see Fig. 4). Also, if an external field is included in the analysis, these mean-field approximations predict an induced ferromagnetic or ferrimagnetic moment, but by construction, they are unable to capture phases III, IV, and the zero-field “ln 72” phase in the rich phase diagram presented in Sec. IV.

- 
- <sup>1</sup> M. E. Zhitomirsky, Phys. Rev. B **67**, 104421 (2003).
  - <sup>2</sup> M. E. Zhitomirsky and H. Tsunetsugu, Phys. Rev. B **70**, 100403(R) (2004).
  - <sup>3</sup> O. Derzhko and J. Richter, Phys. Rev. B **70**, 104415 (2004).
  - <sup>4</sup> S. V. Isakov, K. S. Raman, R. Moessner, and S. L. Sondhi, Phys. Rev. B **70**, 104418 (2004).
  - <sup>5</sup> H. Aoki, T. Sakakibara, K. Matsuhira, and Z. Hiroi, J. Phys. Soc. Jpn. **73**, 2851 (2004).
  - <sup>6</sup> M. Gonzalez, F. Cervantes-Lee, and L. W. ter Haar, Mol. Cryst. Liq. Cryst. **233**, 317 (1993).
  - <sup>7</sup> S. Maruti and L. W. ter Haar, J. Appl. Phys **75**, 5949 (1993).
  - <sup>8</sup> M. Mekata, M. Abdulla, T. Asano, H. Kikuchi, T. Goto, T. Morishita, and H. Hori, J. Magn. Magn. Matt. **177**, 731 (1998).
  - <sup>9</sup> J. Strečka, J. Magn. Magn. Matt. **316**, e346 (2007).
  - <sup>10</sup> D. X. Yao, *Invariant Theory of Time-Dependent Quantum Systems and Ising Model on Triangular Kagome Lattice*, Master's thesis, Zhejiang University, Hangzhou, China (1998).
  - <sup>11</sup> J. Zheng and G. Sun, Phys. Rev. B **71**, 052408 (2005).
  - <sup>12</sup> Y. L. Loh and E. W. Carlson, Phys. Rev. Lett. **97**, 227205 (2006).
  - <sup>13</sup> Y. L. Loh, E. W. Carlson, and M. Y. J. Tan, Phys. Rev. B **76**, 014404 (2007).
  - <sup>14</sup> A. Galluccio, M. Loeb, and J. Vondrak, Phys. Rev. Lett. **84**, 5924 (2000).
  - <sup>15</sup> G. H. Wannier, Phys. Rev **79**, 357 (1950).
  - <sup>16</sup> K. Kano and S. Naya, Prog. Theor. Phys. **10**, 158 (1953).
  - <sup>17</sup> P. W. Kasteleyn, J. Math. Phys. **4**, 287 (1963).
  - <sup>18</sup> M. E. Fisher, J. Mod. Phys. **7**, 10 (1966).
  - <sup>19</sup> T. Horiguchi, K. Tanaka, and T. Morita, J. Phys. Soc. Jpn. **61**, 64 (1992).
  - <sup>20</sup> R. Moessner, S. L. Sondhi, and P. Chandra, Phys. Rev. Lett. **84**, 4457 (2000).
  - <sup>21</sup> R. Moessner and S. L. Sondhi, Phys. Rev. B **63**, 224401 (2001).
  - <sup>22</sup> M. Udagawa, M. Ogata, and Z. Hiroi, J. Phys. Soc. Jpn. **71**, 2365 (2002).
  - <sup>23</sup> R. Moessner and S. L. Sondhi, Phys. Rev. B **68**, 064411 (2003).
  - <sup>24</sup> O. J. Heilmann and E. H. Lieb, Commun. Math. Phys. **25**, 190 (1972).
  - <sup>25</sup> J. R. Heringa and H. W. J. Blöte, Phys. Rev. E **57**, 4976 (1998).
  - <sup>26</sup> W. Krauth and R. Moessner, Phys. Rev. B **67**, 064503 (2003).
  - <sup>27</sup> A. W. Sandvik and R. Moessner, Phys. Rev. B **73**, 144504 (2006).
  - <sup>28</sup> T. Takagi and M. Mekata, J. Phys. Soc. Jpn. **62**, 3943 (1993).
  - <sup>29</sup> J. Stephenson, J. Math. Phys. **5**, 1009 (1964).
  - <sup>30</sup> J. Stephenson, J. Math. Phys. **11**, 413 (1970).
  - <sup>31</sup> K. Husimi and I. Syozi, Prog. Theor. Phys. **5**, 177 (1950).
  - <sup>32</sup> K. Husimi and I. Syozi, Prog. Theor. Phys. **5**, 341 (1950).
  - <sup>33</sup> The erroneous numerical result in Wannier's original paper (0.3383 $k_B$ ) is often quoted, although it was corrected in an erratum 23 years later.<sup>38</sup>
  - <sup>34</sup> R. J. Baxter, J. Phys. A **13**, L61 (1980).
  - <sup>35</sup> I. Syozi, “in *Phase Transitions and Critical Phenomena*, Domb and Green (eds), vol. 1,” (1972).
  - <sup>36</sup> A. Sütö, Z. Phys. B **44**, 121 (1981).
  - <sup>37</sup> S. M. S. Ateca and W. ter Haar, J. Magn. Magn. Matt.

**147**, 398 (1995).

<sup>38</sup> G. H. Wannier, Phys. Rev. B **7**, 5017 (1973).

<sup>39</sup> Note that the enclosed  $a$ -trimer is *not* restricted to a par-

ticular  $S_z$  subspace, as shown in Fig. 7(b).